Unsteady Ventilation in a Scaled Room Model with Swirl Ceiling Diffusers

Eva Mesenhöller [a,b], *Steffen* Jacobs [a,c], *Peter* Vennemann [a], *Jeanette* Hussong [c]

[a] Department of Energy, Building Services, and Environmental Engineering, FH Münster, Steinfurt, Germany, eva.mesenhoeller@fh-muenster.de, s.jacobs@fh-muenster.de, vennemann@fh-muenster.de.

[b] Chair of Hydraulic Fluid Machinery, Faculty of Mechanical Engineering, Ruhr-University Bochum, Bochum, Germany.

[c] Institute for Fluid Mechanics and Aerodynamics, Faculty of Mechanical Engineering, Technical University Darmstadt, Darmstadt, Germany, hussong@sla.tu-darmstadt.de.

Abstract. Mechanical ventilation of buildings is generally based on steadily operating systems. This field is well known and established. But, an approach based on time-varied supply flow rates might improve indoor air quality, comfort, and energy consumption. Typical time-scales of the variation are in the order of seconds or minutes. Until now, the effects of unsteady ventilation scenarios are not fully described and so, reliable dimensioning rules are missing. Hence, with a better understanding of the flow in unsteady ventilation, systems can be calculated and optimised. To understand the effective mechanisms and derive functional relations between the flow field and variation parameters, full-field optical flow measurements are executed with a particle image velocimetry (PIV) system. Experiments are conducted under isothermal conditions in water in a small-scale room model (1.00 m × 0.67 m × 0.46 m) with two swirl ceiling diffusers, Reynolds-scaling assures similarity. In a series of experiments, the effects of different unsteady ventilation strategies on the flow fields are investigated and compared to steady conditions with the same mean exchange rate. Mean exchange rates, signal types, periods, and amplitudes are varied. Time-averaged normalised velocity fields already indicate notable differences between steady and unsteady cases especially for lower exchange rates: the distribution is more homogeneous in unsteady scenarios compared to steady conditions, and low-velocity areas are reduced while the mean velocity of the room increases. So, unsteady ventilation might be beneficial in terms of improved ventilation and energy savings in partial-load operation. Fast Fourier Transformation (FFT) analyses of the mean velocity for each field over the whole series detect the main frequency of the volume flow variation. By dividing the velocity field into smaller areas, this main frequency is still detected especially in the upper part of the room, but side frequencies play a role in the room as well.

Keywords. unsteady ventilation, PIV, room airflow, mixing ventilation.
DOI: https://doi.org/10.34641/clima.2022.200

1. Introduction

Ventilation and air conditioning are an important technology in modern, highly-insulated and airtight buildings – not only about preventing mould by ensuring a sufficient air exchange but also about maintaining good indoor air quality for occupants. As a result of the Covid-Pandemic, the focus has shifted to ventilation and air conditioning systems and hygienically necessary air exchange rates to prevent the virus concentration in the occupied zone from rising above a critical level at which occupants can become infected. But also climate change and resulting higher outdoor temperatures are contributing factors for an increasing demand for air conditioning in buildings. However, despite improved building standards and well-established approaches to reduce the energy consumption of ventilation and air conditioning systems, such as heat recovery, speed-controlled fans, or demand-controlled ventilation rates, the energy consumption for ventilation and air conditioning in buildings is increasing [1–3].

A newer approach with potential for reducing the energy consumption of ventilation and air conditioning could be found in so-called unsteady ventilation systems, where supply flow rates or temperatures are varied in short time intervals (seconds, minutes). Kaup [4, 5] for example

registered energy savings in the range of up to 20 % (heat) and up to 40 % (electricity) while improving the room airflow and comfort. Additionally, energy savings can be achieved in scenarios with high temperatures, as set-point temperatures can be increased because occupants still feel comfortable at higher temperatures due to the air movement (e.g. [6–8]). Scientific and industrial studies indicate that this mode of operation can furthermore improve comfort (e.g. [9–11]), mixing, and velocity/ temperature/pollutant distributions (e.g. [12–15]). More detailed descriptions of the state of the art in science and technology at national and international level are summarised in a review article [16]. Complete scientific explanations for the observed effects have not yet been derived. A first explanatory attempt for enhanced mixing through vortex structures was reported by Sattari [13] and Fallenius [17]. A wide use in practice is currently prevented due to the lack of design rules, standardised systems, or suitable software. Hence, the identification and explanation of effective mechanisms and functional relations between parameters and room airflow are essential for developing such design rules and calculation bases.

Room airflows are usually analysed by punctual measurements of velocities or temperatures. So, information about conditions in the room is only of a discrete type, or simply visualised with smoke gas experiments. Through full-field measurements using PIV combined with computational fluid dynamics (CFD), flow structures can be recorded and analysed entirely with a high level of detail at different points in time. Measurement and simulation data confirm and support each other. Statistical design of experiments offers the possibility not only to find the effects of single parameters on the flow, but also to uncover interactions between different parameters. With the help of the results from both approaches, a better understanding of room airflow in unsteady ventilation is to be gained to derive practice recommendations.

The purpose of this article is to describe findings from two-dimensional PIV-measurements on flow structures and velocity fields in a scaled model room under isothermal conditions and to draw comparisons between steady and unsteady modes of operation at different mean exchange change rates. The unsteady mode of operation was generated by varying the supply volume flow over time, using two different signal types. In addition, diffuser types, cycle durations, and amplitudes of the signals were varied. Pulse lengths of high and low volume flows were of equal duration. The focus of these measurements is on the effects of previously described operating parameters on the flow field in the entire room, especially the large-scale structures. Inlets used in the investigations described in this article were scaled swirl ceiling diffusers. Within the scope of the investigations, the following questions are to be clarified:

- Do flow structures in unsteady ventilation differ from those in steady-state ventilation?
- Do velocities and flow structures follow the volume flow variation?
- Is the velocity distribution more homogeneous in the unsteady case?

Finally, the article shall give hints on where to set the focus in future experiments.

2. Research Methods

2.1 Scale Model

For the investigation of the entire flow field in the room with a PIV-system, smaller dimensions than in real facilities must be considered. Scale models are an established method in fluid mechanics to guarantee similar conditions. Here, relevant dimensionless parameters have to be kept constant in real and scaled setups. There are no heat sources or temperature differences between supply and room in the experimental setup, leading to almost isothermal conditions without buoyancy effects. Hence, the relevant dimensionless parameter is the Reynolds-number according to Posner et al. [18], and Anderson and Mehos [19]. Thus, it is possible to analyse the effects of different unsteady ventilation strategies on the "basic" flow structures.

The model room (1.00 m × 0.67 m × 0.46 m) is geometrically related to the air-conditioning test room at FH Münster (6.22 m × 4.19 m × 2.86 m). Water is used instead of air in the scaled model. As dimensions and kinematic viscosity decrease in the model, velocities and times have to be multiplied by the factors from Tab. 1 to obtain quantities in the non-scaled room. Reynolds numbers in the experiments mentioned are between 14 900 and 22 300.

Tab. 1 – Scale factors (test room / scale model).

	dimensions	time	velocity	kin. viscosity
factor	6.25	2.73	2.29	14.33

Two supply inlets are symmetrically arranged in the ceiling at the room's centre line. Five smaller return outlets are located in the room's rear wall above the floor. The room is placed inside a 1 m³ water tank. A pump in the tank transports the water through pipes and valves from the tank to the supply inlets. Flow rates can be regulated by three valves, where the pneumatic valve generates the flow rate variations in unsteady cases. Magnetic-inductive flow metres in each supply pipe measure the flow rates. Valves and flow metres are connected to a PLC control and flow rates are recorded during PIV-measurements. The setup is shown in Fig. 1. 3D-printed models of real swirl ceiling diffusers are used as inlets with an effective opening area of 0.0011 m². The pipe diameter is constantly reduced with 3D-printed nozzles in front of the diffusers.
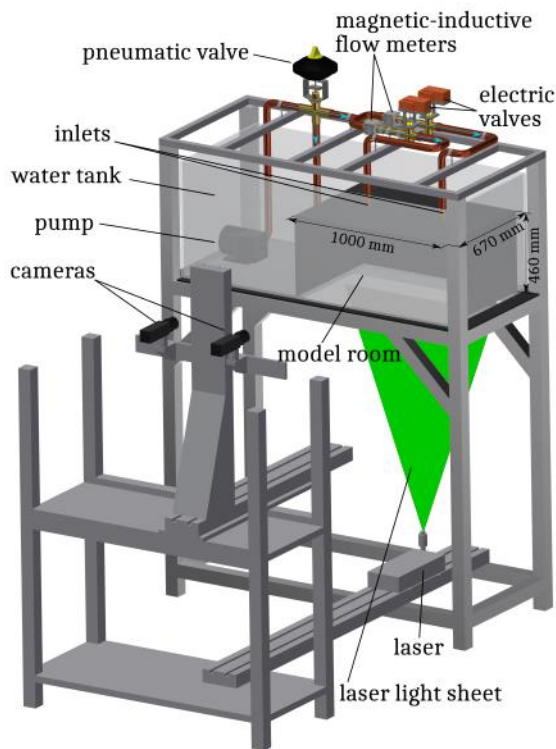
Fig. 1 – Experimental setup. PIV-system consisting of two cameras in front of the model room (one for each half of the room) and a laser under the water tank generating a light sheet. Seeded water is pumped through the pipe system to the diffusers in the ceiling of the model room. A pneumatic valve creates flow rate variations. Blue arrows indicate the flow direction.

2.2 Particle Image Velocimetry (PIV)

Two-dimensional PIV is used to investigate the flow field in the model room. It is a non-invasive, optical measuring technique with which entire flow fields can be analysed. The flow has to be seeded with small particles. The basic principle of PIV is described as follows [20, 21]: a light source generates two flashes to illuminate particles inside a measurement plane and a camera takes pictures of the particles simultaneously to the flashes. Simultaneity is guaranteed by a timing unit. The images are divided into smaller areas, so-called interrogation windows. Inside these interrogation windows, particle patterns in the image pairs are evaluated by cross-correlation algorithms to obtain the local shift. Velocities are then calculated by the known time interval between the acquisitions, resulting in a velocity field with high resolved information that can be used to derive further quantities.

In the experiments, the light source is a 200 mJ double-pulsed Nd:YAG laser (Litron Nano PIV L) with a wavelength of 532 nm. Images are acquired by two side-by-side arranged 5 Mpx double-frame CCD-cameras (LaVision Imager Pro SX 5M) with 7 Hz acquisition rate. Wide-angle lenses (Nikon AF Nikkor 35mm 1:2D) were used. The magnification factor was 4.33458 px mm^{-1}. Vestosint 1101 by Evonik was used as tracer particles (particle size distribution: 100 % <250 μm, ≥45 % <100 μm, ≤2 % <32 μm). The

measurement plane is located in the centre line of the room right under the supply inlets, as can be seen in Fig. 1. A 90° deflection element and light-sheet optics (f=-9.7 mm) were used to generate the measurement plane. The time between the exposures of the first and the second frame depends on the flow properties; here it is between 9 ms (maximum exchange rate) and 15 ms (minimum exchange rate). This time was chosen as a compromise between resolving higher velocities at the diffusers and lower velocities in the room. If the chosen time delay is too long, higher velocities cannot be calculated since the particles have moved out of the interrogation window, but lower velocities can be resolved with good accuracy. This is also a problem if there is a high out-of-plane motion. If the chosen time delay is too short, lower velocities cannot be resolved any more as the particles seem to have no motion, but higher velocities can be calculated. The setup was calibrated by using LaVision's software DaVis 8.4 with a calibration plate of the size of the measurement plane placed at the location of the light sheet. To guarantee a correct mapping of the processed vector fields, there has to be an overlap area acquired by both of the cameras with a size of at least 10 % of the measurement width. The size of the interrogation windows is decreased from 64 px × 64 px to 16 px × 16 px during the multi-pass processing procedure. The overlap was 50 % and two passes were selected for each step. Spurious vectors in the velocity fields were identified by using the universal outlier detection by Westerweel and Scarano [22] and removed during multi-pass processing. In the last step, the processed vector fields of both cameras are merged to create one vector field for the whole model room.

2.3 Experimental Design

Five different factors were identified for possibly influencing the flow; three of a quantitative nature (a-c), and two of a qualitative one (d, e):
a) offset (mean supply flow rate) (OFF)
b) amplitude (AMP)
c) cycle duration (CYC)
d) inlet type (INL)
e) signal type (SIG)
Test planning is based on fractional factorial design of experiments, as it enables both main effects and twofold interactions between factors to be identified. Higher-order interactions are negligible [23]. A 2^{5-1} design was chosen with two settings for each factor, extended by centre point testing. For the full study, 16 different experiments, completed by eight centre point tests (each combination of qualitative factors tested twice at the centre point settings of the quantitative ones) had to be performed to identify possible deviations from linearity. So there were three different settings for each quantitative factor and two for the qualitative ones. This article presents one part of the complete study. Tab. 2 shows the relevant extract of the experimental design and related factor settings.

Tab. 2 – Overview of the experimental design for experiments in the scale model. - and + are factor settings of the 2^{5-1} design, o is the centre point setting.

No.	OFF	AMP	CYC	INL	SIG
-	3.33 m³h⁻¹	0.25	0.05	nozzle	sine
o	4.16 m³h⁻¹	0.5	0.125	/	/
+	4.99 m³h⁻¹	0.75	0.2	swirl	square
1	-	-	-	+	-
2	-	-	+	+	+
3	-	+	-	+	+
4	-	+	+	+	-
5	+	-	-	+	+
6	+	-	+	+	-
7	+	+	-	+	-
8	+	+	+	+	+
9	o	o	o	+	-
10	o	o	o	+	+
11	o	o	o	+	-
12	o	o	o	+	+

Tab. 3 – Actual settings for factors AMP and CYC for different offsets in the scale model.

OFF [m³h⁻¹]	AMP [m³h⁻¹]			CYC [s]		
	-	o	+	-	o	+
3.33	0.67	-	2.00	16.5	-	66.0
4.16	-	0.92	-	-	33.0	-
4.99	0.25	-	0.76	11.0	-	44.0

Additionally, measurements of the corresponding steady scenarios with comparable mean exchange rates were conducted. The offset was derived by typical mean exchange rates, respectively 4 h⁻¹, 5 h⁻¹ and 6 h⁻¹ in non-scaled dimensions. The corresponding nominal time constants in the scaled model are 330 s, 264 s, and 220 s. All values in Tab. 2 are based on the scaled model. Parameters for the amplitude in Tab. 2 represent the proportion of the smallest difference between offset value and the total maximum/ minimum of the system to realize the maximum possible fluctuation range, see Fig. 2 for a graphical explanation of the procedure.
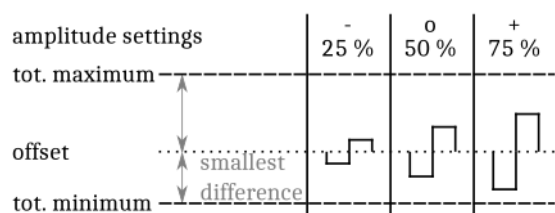

Fig. 2 – Amplitude definition for the settings -, o, and + from Tab. 2. Percentage values refer to the proportion of the smallest difference between offset and total minimum/maximum.

Parameters for the cycle duration in Tab. 2 indicate the proportion of the nominal time constant used for the variation, analogous to the definition of van Hooff and Blocken [14]. Using the proportions from Tab 2, the actual settings for amplitude and cycle duration in Tab. 3 can be calculated.

3. Results and Discussion

3.1 Prerequisites

For sine wave signals, the acquisition was started at the offset (on the downward slope of the wave), and for square waves, it was started at the beginning of the low period. Spurious vectors were removed before further analyses of the vector fields and replaced by the median of their neighbours. The definition of the occupied zone is based on DIN EN 16798-3 (0.05-1.8 m height, 0.5 m to walls): It is located between $y/H=-0.98$ and $y/H=-0.37$ and $x/L=0.08$ and $x/L=0.92$, where y is the actual height and H is the full height of the room and x is the actual length and L is the full length of the room.

3.2 Time-Averaged, Normalised Velocity Fields

To ensure comparability between the cases, the following velocity fields are presented in normalised form. The normalisation is based on the time-averaged velocity at the supply inlets during the measurements. Colours indicate the velocity magnitude and arrows show the flow direction. To ensure good visibility of the lower velocities in the model room, maximum normalised velocity in the contour plots was set to $u/u_0=0.15$, where u is the actual velocity and u_0 is the mean velocity at the inlets. Time-averaged velocity fields in steady cases are based on 250 single pictures, and in unsteady cases on the number of pictures acquired during three full cycle durations.

Fig. 3, 4 and 5 show the time-averaged normalised velocity fields at minimum, medium and maximum mean exchange rates; the reference cases with steady conditions are shown in subfigures a). Mean normalised velocity fields of all cases presented show expectable flow structures: the inlet flow radially spreads out under the ceiling after exiting the swirl diffusers in the model room. The mean flow direction changes at the walls and in the middle of the room where the jets merge. Differences between the average velocity fields of steady and unsteady scenarios are present especially in case of minimum exchange rates, as can be seen in Fig. 3.
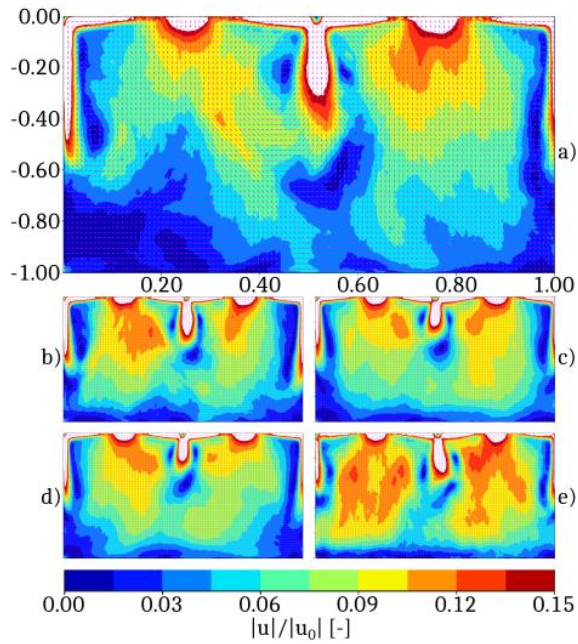
Fig. 3 – Time-averaged, normalised velocities for minimum exchange rates: a) steady case Ref. 1, b) Exp. No. 1, c) Exp. No. 4, d) Exp. No. 2, e) Exp. No. 3.
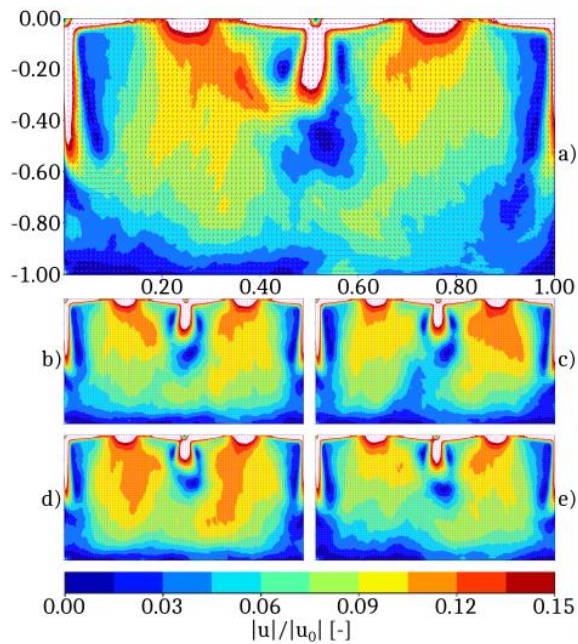

Fig. 4 – Time-averaged, normalised velocities for medium exchange rates: a) steady case Ref. 2, b) Exp. No. 9, c) Exp. No. 11, d) Exp. No. 10, e) Exp. No. 12.
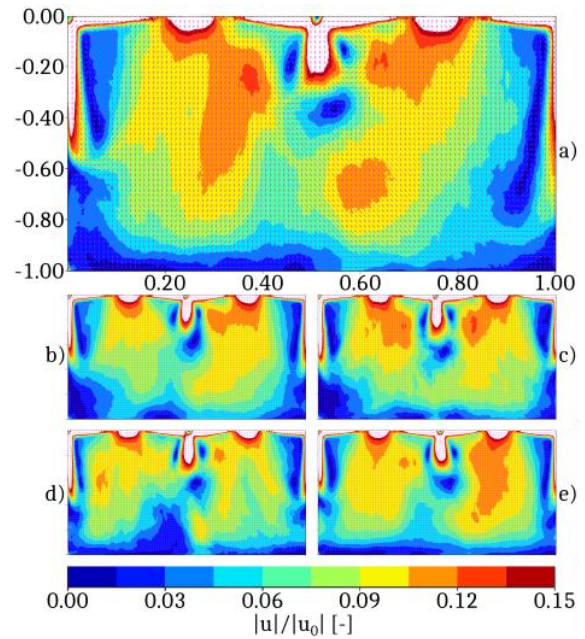

Fig. 5 – Time-averaged, normalised velocities for maximum exchange rates: a) steady case Ref. 3, b) Exp. No. 6, c) Exp. No. 7, d) Exp. No. 5, e) Exp. No. 8.

Tab 4 presents a summary of the mean velocities at the inlets (v_{in}), mean (v_{mean}), and median velocity (v_{median}), the difference between 95 % percentile and 5 % percentile (p_{95-5}) of the whole velocity field, and the relative deviation of p_{95-5} in unsteady cases related to the steady cases (Δ).

Tab. 4 – Statistical data of time-averaged, normalised velocity fields; Exp. No. refer to Tab. 2.

No.	v_{in} [ms^{-1}]	v_{mean} [ms^{-1}]	v_{median} [ms^{-1}]	p_{95-5} [ms^{-1}]	Δ [%]
Ref.1	0.43	0.066	0.059	0.129	-
1	0.43	0.073	0.069	0.126	-2.33
2	0.43	0.072	0.071	0.111	-13.95
3	0.43	0.085	0.088	0.110	-14.73
4	0.43	0.073	0.073	0.114	-11.63
Ref.3	0.64	0.080	0.079	0.116	-
5	0.64	0.075	0.075	0.118	+1.72
6	0.64	0.075	0.074	0.115	-0.86
7	0.64	0.079	0.080	0.124	+6.90
8	0.64	0.080	0.080	0.116	0.00
Ref.2	0.54	0.073	0.069	0.117	-
9	0.54	0.076	0.076	0.117	0.00
10	0.53	0.080	0.083	0.110	-6.00
11	0.54	0.075	0.074	0.120	+2.56
12	0.54	0.072	0.071	0.114	-2.56

Mean and median velocities increase for all unsteady cases with a minimum exchange rate compared to the steady scenario. This behaviour can also be found for medium exchange rates, except for Exp. No. 12. The highest increase can be recognised for Exp. No. 3 (minimum exchange rate), and Exp. No. 10 (medium mean exchange rate). For maximum exchange rates, the velocities tend to decrease under unsteady conditions, except for Exp. No. 8. Taking the difference between 95 % percentile and 5 % percentile into account, a reduction can be recognised for unsteady cases with a minimum exchange rate. This can be interpreted as a more homogeneous velocity distribution under unsteady conditions as the range of velocities gets smaller. For medium and maximum exchange rates, reductions can be detected only for some cases.

3.3 Frequency Analysis of Instantaneous Velocity Fields

Instantaneous velocity fields are analysed via FFT to check for main and secondary frequencies. The sampling frequency of 7.0 Hz was considerably higher than the frequency required according to the Nyquist-Shannon theorem to correctly detect the frequencies of the volume flow variations. The following questions should be answered after analysing the frequencies of the velocity fields:

- Is it possible to detect the variation frequency in the mean velocity of the whole velocity field?
- In which areas of the velocity field are the main frequencies detected strong?

For answering these questions, the following analyses were performed:

- FFT-analysis of the series of mean velocities in each velocity field
- FFT-analysis of the series of mean velocities in small areas in each velocity field (in the further course called "regional FFT")

In a first step, a mean velocity was calculated for each instantaneous velocity field of the full series and analysed via FFT. As expected, steady scenarios did not show remarkable magnitudes, while unsteady scenarios did. The frequency of the flow rate variations was detected as the frequency with the highest magnitudes in all cases except for Exp. No. 5, see Tab 5. In Exp. No. 5, the magnitudes themselves were of a low level (between 0.13 and 0.17) and there is a region without a clear peak between the frequencies 0.030 s^{-1} and 0.121 s^{-1}. A low peak level of the FFT-results was also present for Exp. No. 1, 3, 6, and 7 with the highest magnitudes smaller than 1.0. In experiments with the same cycle durations, magnitudes of the FFT were higher for cases with higher amplitudes. Experiments with the same mean exchange rates showed the highest magnitudes for those cases with longer cycle durations. Magnitudes for all centre point experiments varied between 1.98 and 2.50 with slightly higher peaks for square wave signals.

Tab. 5 – Highest magnitudes and related frequencies of the FFT-analyses of mean velocities.

No.	Magnitude [-]	Frequency [s^{-1}]
1	0.35	0.061
2	5.79	0.015
3	0.96	0.061
4	12.54	0.015
5	0.17	0.061
6	0.87	0.023
7	0.42	0.091
8	4.14	0.023
9	1.98	0.030
10	2.27	0.030
11	2.17	0.030
12	2.50	0.030

Results of the regional FFT-analyses with the highest peaks for each mean exchange rate (see Tab. 5) are displayed in Fig. 6. Velocity fields were divided into small regions of the size of 20 mm × 18.4 mm (50 boxes in x-direction and 25 boxes in y-direction). Mean velocities per box were calculated for the whole series and FFT-analyses were performed for each region. The colours of the boxes in Fig. 6 indicate the magnitude of the FFT for the main frequency. Highest magnitudes are detected in the upper centre of the room in the merging area of the jets, but the occupied zone is also influenced by the variation frequency. Secondary frequencies may influence other parts of the room.
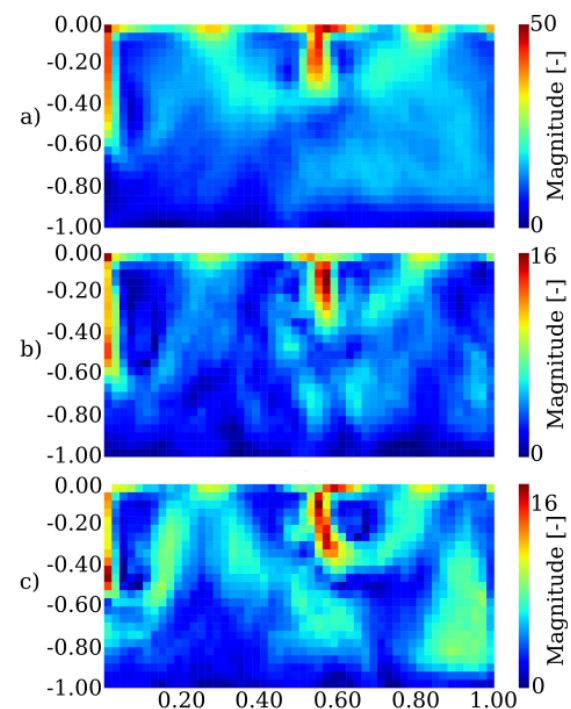

Fig. 6 – Regional magnitudes of the main frequency: a) Exp. No. 4, b) Exp. No. 12, c) Exp. No. 8.

4. Conclusions

Average velocity fields of steady and unsteady cases already showed differences in local velocities. Single velocity fields of all steady reference cases did not vary over time and showed comparable structures to average velocity fields, which is also proved by a constant standard deviation. Single velocity fields of the unsteady cases differed in time, depending on the conditions of the supply flow rate. The frequency of the supply flow rate variations could also be detected as the main frequency in the velocity changes. Consequently, it is inevitable, that instantaneous velocity fields and not averaged values have to be taken into account for analysing the effects of unsteady ventilation scenarios. This kind of ventilation seems to have a stronger impact under lower mean exchange rates.

Taking into account the results presented in this article, the three main questions asked in the introduction can be answered as follows:
1. Do flow structures in unsteady ventilation differ from those in steady-state ventilation?

Flow structures in the room are influenced by supply flow rate variations, which can already be seen in time-averaged velocity fields, especially for minimum exchange rates. Here, also the lower part of the room seems to be affected by the variable flow rates, as velocities in unsteady cases increase in this part.
2. Do velocities and flow structures follow the volume flow variation?

FFT analyses of the velocity fields detect the frequency of the flow rate variation as the dominating frequency in the room, but secondary frequencies can be identified in some cases as well. Regional FFT shows that especially the merging zone of the jets is affected by the variation frequency.
3. Is the velocity distribution more homogeneous in unsteady cases?

Time-averaged velocity fields indicate a more homogeneous velocity distribution and higher mean velocities, especially for minimum exchange rates. In this article, a difference between 5 % and 95 % percentile is used to derive a measure of homogeneity. This quantity was compared to steady conditions and varied between -2.33 % and -14.73 % for minimum exchange rates meaning that the spread of velocities decreases.

5. Outlook

This study gives first indications that the effects of supply flow rate variations are stronger in lower exchange rates. This can be inferred by comparing the difference in percentiles and mean velocities to the reference cases. If the greatest effects occur at lower exchange rates, this would support an improvement of the ventilation in part-load operation and energy-savings. In further investigations, the focus should therefore be set on low exchange rates.

Furthermore, it is necessary to derive functional relations between unsteady ventilation scenarios and flow quantities to draw conclusions that are beneficial for a wider practical application of unsteady ventilation scenarios. Subsequently, the experimental data will be used to validate a CFD model. With the help of this model, further parameter studies will be carried out via simulations under isothermal conditions. Effects and interactions of factors will be evaluated after finishing the whole series of experiments to draw conclusions, derive functional relations, and develop dimensioning rules or application recommendations. Effects of contrary supply flow rates and non-equally timed high and low periods should also be considered in future experiments.

The results presented in this article indicate the necessity of using time-resolved measurements, e.g. for vortex tracking. As the flow has a strong three-dimensional property, three-dimensional velocity measurements using particle tracking velocimetry (PTV) would help to gain a deeper understanding of the mechanisms and development of flow structures in the ventilated room.

6. References

[1] Diefenbach N., Cischinsky H., Rodenfels M., et al. Datenbasis Gebäudebestand: Datenerhebung zur energetischen Qualität und zu den Modernisierungstrends im deutschen Wohngebäudebestand. IWU Darmstadt. 2010.

[2] Bettgenhäuser K., Boermans T., Offermann M., et al. Klimaschutz durch Reduzierung des Energiebedarfs für Gebäudekühlung. UBA Dessau-Roßlau. 2011.

[3] Koch M., Kenkmann T., Winger C., et al. Klimatisierungsbedarf und dafür abgerufener Stromverbrauch für Wohngebäude in Deutschland von 2020 bis 2050. Öko-Institut e.V. Freiburg. 2017.

[4] Kaup C. Impulslüftung für bessere Luftqualität. Instationäre RLT-Anlage zur intermittierenden Raumlüftung. Tech am Bau. 2012; 43: 54–59.

[5] Kaup C. Höhere Luftqualität mit geringerer Luftmenge. TGA Fachplaner. 2013; 1–8.

[6] Huang L., Ouyang Q., Zhu Y. Perceptible airflow fluctuation frequency and human thermal response. Build Environ. 2012; 54: 14–19.

[7] Kabanshi A. Experimental study of an intermittent ventilation system in high occupancy spaces. 2017.

[8] Zhou X., Ouyang Q., Lin G., et al. Impact of dynamic airflow on human thermal response. Indoor Air. 2006; 16: 348–355.

[9] Luo M., Yu J., Ouyang Q., et al. Application of dynamic airflows in buildings and its effects on perceived thermal comfort. Indoor Built Environ. 2018; 27: 1162–1174.

[10] Wigö H. Effects of intermittent air velocity on thermal and draught perception -A field study in a school environment. Int J Vent. 2013; 12: 249–255.

[11] Zhu Y., Luo M., Ouyang Q., et al. Dynamic characteristics and comfort assessment of airflows in indoor environments: A review. Build Environ. 2015; 91: 5–14.

[12] Lichtner E., Kriegel M. CFD-Studien zur intermittierenden Belüftung von Räumen – Potenzialanalyse und vereinfachte Modellierung. In: BauSIM. 2014; 536–540.

[13] Sattari A. Investigations of Flow Patterns in Ventilated Rooms Using Particle Image Velocimetry. KTH Royal Institute of Technology. 2015.

[14] van Hooff T., Blocken B. Mixing ventilation driven by two oppositely located supply jets with a time-periodic supply velocity: A numerical analysis using computational fluid dynamics. Indoor Built Environ. 2020; 29: 603–620.

[15] Backes C., Kaup C. Möglichkeit zur Luftmengenreduzierung. Steigerung der Effektivität der Verdünnungsströmung durch Intermittierende Raumlüftung - Teil 1. HLH. 2016; 67: 17–21.

[16] Mesenhöller E., Vennemann P., Hussong J. Unsteady room ventilation – A review. Build Environ. 2020; 169: 106595.

[17] Fallenius BEG., Sattari A., Fransson JHM., et al. Experimental study on the effect of pulsating inflow to an enclosure for improved mixing. Int J Heat Fluid Flow. 2013; 44: 108–119.

[18] Posner JD., Buchanan CR., Dunn-Rankin D. Measurement and prediction of indoor air flow in a model room. Energy Build. 2003; 35: 515–526.

[19] Anderson R., Mehos M. Evaluation of indoor air pollutant control techniques using scale experiments. In: ASHRAE Conference IAQ. 1988; 193–208.

[20] Adrian RJ., Westerweel J. Particle image velocimetry. Cambridge University Press. 2011.

[21] Raffel M., Willert C., Wereley ST., et al. Particle Image Velocimetry (3rd ed.). Springer. 2018.

[22] Westerweel J., Scarano F. Universal outlier detection for PIV data. Exp Fluids. 2005; 39: 1096–1100.

[23] Kleppmann W. Versuchsplanung - Produkte und Prozesse optimieren (8th ed.). Hanser . 2013.

Data Statement